B. M. JOVIĆ[1], V. D. JOVIĆ[1], U. Č. LAČNJEVAC[1], Lj. GAJIĆ-KRSTAJIĆ[2], N. V. KRSTAJIĆ[3]*

[1]University of Belgrade, Institute for Multidisciplinary Research, Belgrade, Serbia, [2]Institute of Technical Sciences SASA, Belgrade, Serbia, [3]University of Belgrade, Faculty of Technology and Metallurgy, Belgrade, Serbia

Scientific paper
ISSN 0351-9465, E-ISSN 2466-2585
UDC:620.197.5
doi:10.5937/ZasMat1601136J

Zastita Materijala 57 (1)
136 - 147 (2016)

Electrodeposited Ni-Sn coatings as electrocatalysts for hydrogen and oxygen evolution in alkaline solutions

ABSTRACT

The hydrogen evolution reaction (HER) and the oxygen evolution reaction (OER) were studied at electrodeposited Ni-Sn alloys. All coatings were electrodeposited onto a Ni 40 mesh substrate from a bath containing Ni and Sn ions in the presence of pyrophosphate and glycine. The electrodes were investigated by cyclic voltammetry (CV), scanning electron microscopy (SEM), energy dispersive X-ray spectroscopy (EDS), electrochemical impedance spectroscopy (EIS) and polarization measurements. It was shown that among the increase of the roughness factor of Ni-Sn coatings with the increase of electrodeposition current density, their composition was also responsible for their catalytic activity for both, the HER and the OER. In the potential range of the HER two regions were observed, but none of them was characterized with the linear dependence E vs. log j (Tafel slope). For the OER two Tafel slopes were detected: one of about 60 mV dec^{-1} at lower current densities (up to about 20 mA cm^{-2}) and one of about 120 mV dec^{-1} at higher current densities. Based on the Tafel slopes and EIS results the mechanisms for the HER and OER were proposed and discussed.

***Key words**: H_2 evolution, O_2 evolution, alkaline solution, electrodeposited Ni-Sn alloys.*

1. INTRODUCTION

The HER and the OER are industrially important reactions in water electrolysis. Catalytic activity for the HER in alkaline solutions on electrodeposited Ni-Sn alloys has been first discovered in 1992 in the work of Santos et al. [1]. It was shown that such coatings possess low overvoltage for hydrogen evolution in alkaline solution, although the correlation between the characteristics of the alloys and the ability for the HER has not been discussed. In the work of Yamashita et al. [2] the influence of the electrodeposition conditions (bath composition, temperature, current density etc.) on the morphology of the Ni-Sn alloy coatings and overvoltage for the HER in alkaline solution has been investigated. By changing the deposition current density and concentration of $SnCl_2$ in the pyrophosphate-glycine bath, Ni content in the alloy coatings was changed from 34 to 99 at. %, while the overvoltage for hydrogen evolution was found to be practically independent of the alloy composition in the range 53 - 90 at. %. The morphology of the coatings was found to change from relatively smooth, fine grain structure, at low plating current density, to nodular one appearing as large spherical particles with the diameter of about 15 μm at high plating current density [2]. In the paper by Jović et al. [3], Ni-Sn alloy coatings were electrodeposited onto Ni plate electrodes from the pyrophosphate–glycine bath containing the same concentrations of Sn^{2+} and Ni^{2+} ions (0.1 M) at different current densities and their morphology, chemical and phase compositions were investigated. Four crystalline phases of low crystallinity were detected in total: face centered cubic (*fcc*) Ni phase, hexagonal close packed (*hcp*) Ni_3Sn phase, hexagonal $Ni_{(1+x)}Sn$ ($0 < x < 0.5$) phase adopting NiAs type structure (dominant in most samples) [2,3] and monoclinic Ni_3Sn_4 phase with CoSn type structure. Mainly Ni_3Sn_4 phase (and in small amount Ni_3Sn phase) were detected in the sample deposited at the lowest current density (–2 mA cm^{-2}), while Ni (actually Ni-Sn solid solution with small amount of Sn) and $Ni_{(1+x)}Sn$ ($0 < x < 0.5$)

*Corresponding author: B.M. Jović
E-mail: vlada47@yahoo.com
Paper received: 25. 11. 2015.
Paper accepted: 15. 01. 2016.
Paper is available on the website: www.idk.org.rs/casopis

phases were present in all other samples deposited at –4, –6, –20 and –40 mA cm^{-2}. Their catalytic activities for the HER in 6 M KOH were also investigated. It was shown that the phase composition is responsible for their catalytic activity for the HER on flat samples (–2, –4 and –6 mA cm^{-2}) to some extent, while on rough samples (–20 and –40 mA cm^{-2}) both, phase composition and roughness, influenced the overvoltage for the HER, with the roughness effect being the most pronounced one.

The OER is very sensitive to the nature and structure of the electrocatalysts [4]. Since the reaction takes place at high positive potentials, the problem of corrosion stability of electrocatalysts is often present. It is generally accepted that the Ni-based spinels [5-7] and perovskites [8,9] are good electrocatalysts in alkaline media. Nickel itself is a good electrocatalyst for the OER in alkaline solutions due to its relatively low overvoltage, high corrosion stability and reasonable cost price. Nickel is frequently used as a reference anode material for comparison with new electrocatalysts for the OER in alkaline solutions [10-14]. Problems related to the occurrence of loss of activity of NiOx as an oxygen electrode under prolonged anodic polarization, have prompted numerous investigations [7,15,16] of the influence of various metal oxides (hydroxides) as alloying components on the electrochemical properties of NiO_x. Numerous studies have been devoted to the OER on nickel in alkaline solutions. However, there is no general agreement between the experimentally determined kinetic parameters obtained in different laboratories [17-21]. Certain differences in the values of the Tafel slope in the lower overpotential region are probably due to differences in the structure and composition of the oxide film on Ni. It has been shown that the thermally formed Ni-oxide film exhibited much better electrocatalytic activity than the electrochemically formed oxide film [22].

One of the most important factors that lead to a decrease of the production characteristics of the water electrolysis cell is an increase of the overpotential for the OER on Ni-based anodes with time. This phenomenon is also present on platinum [23] in the potential region of 1.6–2.0 V as well as on iridium [24]. The prevailing opinion is that the initial decline in activity with time is a consequence of the continuous growth of the poorly conductive oxide film [25].

Large number of authors have noted the presence of oxides with O/Ni ratio between 1.7 and 1.9 [26,27]. Therefore, the presence of higher oxides than β-NiOOH (O/Ni = 1.5) is possible. Srinivasan et al. [12] have shown that in the potential range of 1.8–2.0 V the conversion of Ni^{3+} to Ni^{4+} ions takes place with the formation of a nonstoichiometric oxide film composed of Ni^{3+}, Ni^{4+}, OH^- and O_2^- ions. The formation of NiO_2 leads to a significant decrease in electrical conductivity of the film and therefore to a decrease in catalytic activity of the NiO_x anode. The loss of catalytic activity of NiO_x electrode may be reduced by: (a) increasing the operating temperature of the electrolyte, in order to reduce the equilibrium concentration ratio of Ni^{3+}/Ni^{4+} ions in the oxide film [10]; (b) by applying an electrode with a highly developed surface area in order to maintain the anode potential below the critical value of 1.56 V at the required current density (Raney-Ni anodes) [28]; (c) by alloying of Ni-oxides [29–34]; (d) by pigmenting Ni coatings with Ru and/or Ir nanoparticles- composite electrocatalysts [35].

The influence of other metal hydroxides on the electrocatalytic activity of NiO_x anodes has usually been studied using simultaneous electrodeposition of these metal hydroxides with nickel hydroxide from a suitable bath [29–31]. However, binary oxides formed by chemical or thermal method were also investigated [32–34]. In particular, the influence of Co, Mn and Fe hydroxides was investigated [7,29]. Cobalt oxides are widely used as an alloying component in order to improve the electrocatalytic activity and stability of Ni oxide electrodes. Maximum activity is achieved when the Co:Ni ratio is 2:1, due to the formation of the $NiCo_2O_4$ spinel [5]. This spinel is much more active than a simple mixture of oxides of Co and Ni of the same chemical composition [36]. However, $NiCo_2O_4$ is unstable in concentrated solutions of KOH (50%) above 100 °C [37].

The largest increase in electrocatalytic activity was observed in the case when iron oxides were incorporated in the nickel oxide [30]. Kamnev et al. [38] examined the influence of iron hydroxide in the wide potential range and observed three linear parts on the polarization curves. High values of the Tafel slope in the third (most positive) potential region could be explained by a double barrier model for the charge transfer process. Raney-Ni electrodes showed good potentials as electrodes (both as cathodes and anodes) for large scale alkaline water electrolysis. These electrodes were highly efficient for the hydrogen reaction [39]; however, more efficiency was desired for the OER. In this work both, the HER and the OER, were studied at the same Ni-Sn alloy coatings.

2. EXPERIMENTAL

2.1. Electrodeposition of Ni-Sn alloy coatings

Before the electrodeposition of samples, polarization measurements for this process were performed in an electrochemical cell with the Ni 40

mesh electrode (1 cm^2) as working electrode and two Pt counter electrodes of the same dimensions placed parallel to the working electrode. A saturated calomel electrode (SCE), as the reference electrode, connected to the working electrode by means of Luggin capillary was used. Electrodeposition of samples for the analysis was performed in the same cell at the constant current densities in the solution 0.1 M $SnCl_2 \cdot 2H_2O$ + 0.3 M $NiCl_2 \cdot 6H_2O$ + 0.6 M $K_4P_2O_7$ + 0.3 M NH_2CH_2COOH of pH 6.7 at 50°C. The dimensions of samples, as well as counter electrodes, were 2 cm x 1 cm. All chemicals were p.a. quality.

All Ni 40 mesh substrates were only shortly etched in 1:3 mixture of H_2O:HNO_3 and washed with distilled water before the electrodeposition. From the weight difference of samples before and after electrodeposition and alloy compositions determined by the EDS, the current efficiency for each sample was calculated. For the SEM and EDS analysis of coating surface, samples were cut into suitable parts and placed on the graphite tape. For the SEM and EDS analysis of a cross-section, samples were sealed in the epoxy resin and polished down to the alumina suspension of 0.05 μm and kept in an ultrasonic bath for 10 min. to remove traces of polishing alumina.

2.2. Characterization of Ni-Sn coatings

The appearance of the Ni-Sn coatings was investigated by SEM, Tescan VEGA TS 5130MM, while the elemental composition of samples was obtained by EDS analysis performed using the same SEM equipped with an energy dispersive X-ray spectroscopy (EDS) system, INCAPentaFET-x3, Oxford Instruments.

2.3. Electrochemical measurements and solutions

The polarization characteristics for the HER were tested in 32 mas. % NaOH solution in extra pure UV water at 90°C, while the polarization characteristics for the OER were tested in 1 M NaOH solution at 25°C. A three-compartment cell was used: the working electrode of the surface area of approximately 1 cm^2 was placed in a central compartment together with the Luggin capillary; two Pt mesh counter electrodes of larger surface areas were each placed in separate compartments (parallel to the working electrode mesh), so that the oxygen (or hydrogen) evolved at the counter electrodes could not enter the working electrode compartment. The SCE was placed in a side compartment connected to the central one through a bridge and a Luggin capillary, and was kept at room temperature. All values of potential in the text are given versus the SCE. All experiments for all investigated electrodes were performed using a potentiostat Reference 600 and software PHE 200 and DC 105 (Gamry Instruments).

(HER): All samples were first submitted to the HER at a constant current density j = -0.3 A cm^{-2} for 800 s (step 1), followed by conditioning at a certain constant potential for the period of 60 s sufficient to provide a stable current density response (step 2). The value of potential in step 2 was adjusted to produce cathodic current density slightly higher than -0.3 A cm^{-2}. After such pre-electrolysis, polarization curves were recorded by sweeping the potential at 1 mV s^{-1} from the value applied in step 2 to the value of open circuit potential. During the course of the sweeps, potential was automatically corrected for the *IR* drop using the current interrupt technique.

(OER): First polarization curve was recorded by sweeping potential with 1 mV s^{-1} from 0.0 V to 0.7 V, while second one was recorded backwards. This procedure was repeated so that in all cases four polarization curves were recorded. During the course of the sweeps, potential was automatically corrected for the *IR* drop using the current interrupt technique. The first one recorded backwards was used for the analysis.

The EIS measurements were performed with the same potentiostat and EIS 300 software, applying the amplitude of 5 mV RMS in the frequency range from 10 kHz to 0.01 Hz with 20 points per decade. EIS spectra were recorded at different potentials for each sample. The real (Z') and imaginary (Z") components of electrochemical impedance spectra in the Nyquist plot were analyzed using the complex nonlinear least squares (CNLS) fitting program (EIS 300) to simulate the equivalent resistances and capacitances.

3. RESULTS AND DISCUSSION

3.1. SEM-EDS characterization

The results of the SEM analysis of the cross-section of the samples A, B, C, and D (j_d = –10 mA cm^{-2}, –30 mA cm^{-2}, –60 mA cm^{-2}, –100 mA cm^{-2} respectively) are presented in Fig. 1. As can be seen sample A (Fig. 1A), electrodeposited at –10 mA cm^{-2} is flat in comparison with other samples, indicating that electrodeposition of alloy is under mixed, activation-diffusion control. At higher cathodic current densities (region of diffusion controlled electrodeposition and simultaneous hydrogen evolution, B, C and D) rougher deposits were obtained, as shown in Fig. 1B,C,D. The average composition of all samples, determined by the EDS analysis, is presented in Table 1. As can be seen the content of Ni increased from 48 ± 2.4 at.% to 66 ± 3.3 at.%, while the current efficiency

for alloy electrodeposition decreased from 92 ± 4.8 % to 67 ± 3.4 % with the increase of cathodic current density from -10 mA cm^{-2} to -100 mA cm^{-2}. Such behavior is reasonable, since at more negative potentials (increase of cathodic current density) more Ni should be electrodeposited and the current efficiency should be lower due to simultaneous hydrogen evolution. The cross-section of the coating A with the EDS analysis performed at different positions (1–8) is presented in Fig. 1A, with the at.% of Ni obtained by the EDS analysis given in the brackets under the numbers 1–8. As can be seen the content of Ni slightly decreases with increasing the coating thickness for about 7 at.% in total (about 1.5 %). The composition change is the most pronounced up to about half of the deposit thickness (about 20 μm), while at the second half of the deposit constant composition is obtained (45 at.% Ni – 55 at.% Sn), indicating that constant composition could be obtained after certain time of deposition. It should be stated that this is characteristic of all samples, with the Ni content decrease over the cross-section of the deposit being more pronounced for samples deposited at higher cathodic current densities (the change in the Ni content reached about 15 at.% for the rough samples). This is most likely due to increase of the real surface area causing the decrease of cathodic current density and the decrease of cathodic potential of electrodeposition. As can be seen the roughness of samples C and D is much more pronounced, samples are characterized with the presence of large nodules, while the sample B possesses slightly rougher surface than the sample A.

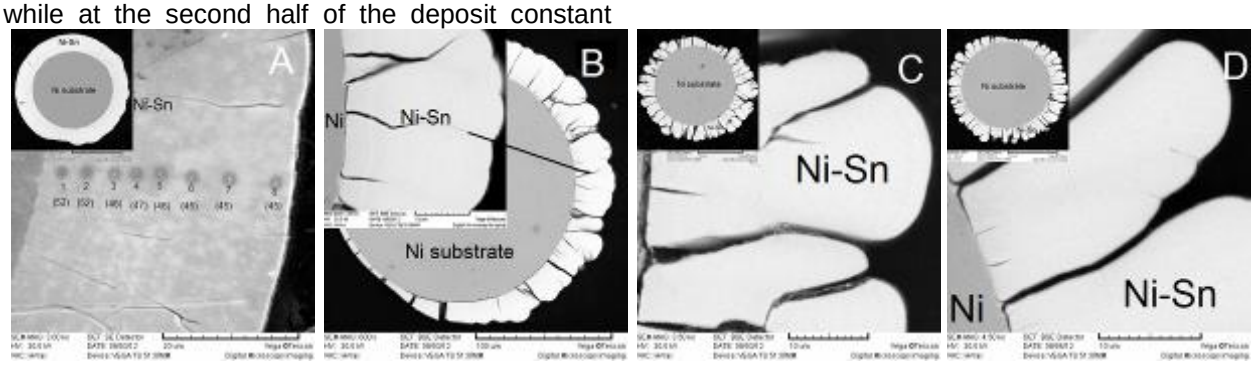

Figure 1 - The results of SEM analysis of the cross-sections of samples A, B, C and D. The cross-section of the sample A with the positions of the EDS analysis (1-8) and content of Ni (at.%) at each point in brackets is presented in (A).

3.2. HER

3.2.1. Polarization curves

Polarization characteristics of the HER onto Ni-Sn coatings in 32 mas. % NaOH at 90^{o}C corrected for the *IR* drop are presented in Fig. 2a for all investigated samples: NiSn(10), j_d = -10 mA cm^{-2}; NiSn(30), j_d = -30 mA cm^{-2}; NiSn(60), j_d = -60 mA cm^{-2}; NiSn(100), j_d = -100 mA cm^{-2}; DN – commercial De Nora's Ni-RuO_2 cathode. The overvoltage for the HER is seen to decrease with increasing deposition current density. This decrease is due to the change in chemical and phase composition of NiSn coatings, as well as due to the change in their morphology, clearly demonstrated in our previous paper [3]. Polarization characteristics for the HER onto commercial DN electrode (Ni-RuO_2 coating deposited onto Ni 40 mesh) are also presented in the same figure. As can be seen in the region of current densities lower than 0.2 A cm^{-2} the overvoltage for the HER onto DN electrode is lower than that on all NiSn samples (Fig. 2a). At higher current densities the overvoltage for the HER onto NiSn samples NiSn(30), NiSn(60) and NiSn(100) is lower than that onto DN (Fig. 2a). Such behavior indicates that rough NiSn coatings could be promising replacement for the commercial DN electrode. The values of current densities recorded at the potential of -1.2 V (at which EIS measurements were performed) for all investigated samples, taken from the polarization curves presented in Fig. 2a, are presented Fig. 2b, while in Fig. 2c are presented values of potentials corrected for the *IR* drop recorded at j = -0.3 A cm^{-2} (taken from the polarization curves presented in Fig. 2a) for all investigated samples. Figs. 2b and 2c show that the DN cathode is more active for the HER at -1.2 V, while at j = -0.3 A cm^{-2} the most active cathode for the HER is NiSn(100) sample (the overvoltage is for about 10 mV lower than that onto commercial DN cathode). All investigated electrodes exhibit high catalytic activity resulting in the current density change for four decades in a very narrow potential range of about 100 mV.

Table 1 - Average compositions and current efficiencies for Ni-Sn alloy samples electrodeposited at different current densities (j_d).

Sample	j_d / mA cm^{-2}	Average at. % Ni	Average at. % Sn	Δm / g	η_j / %
A	–10	48 ± 2.4	52 ± 2.6	0.2812	92 ± 4.8
B	–30	60 ± 3.0	40 ± 2.0	0.2439	86 ± 4.3
C	–60	63 ± 3.1	37 ± 1.8	0.2109	76 ± 3.8
D	–100	66 ± 3.3	34 ± 1.7	0.1800	67 ± 3.4

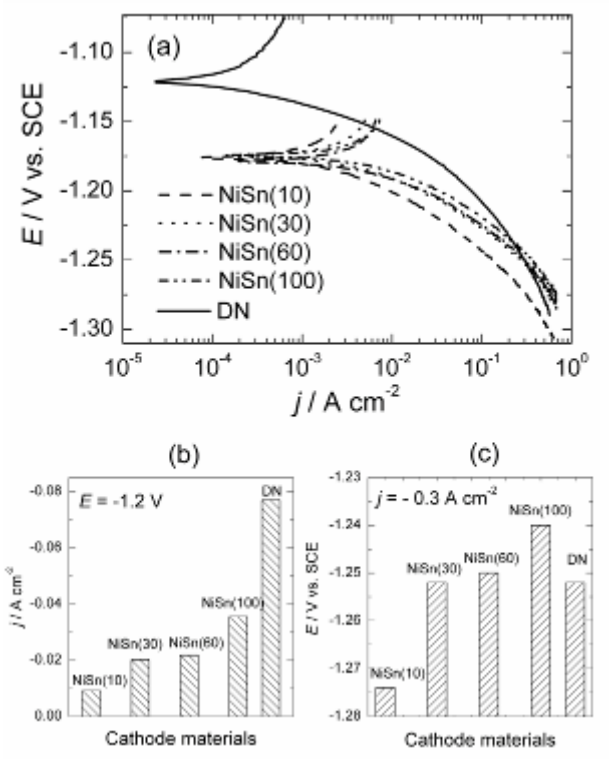

Figure 2 - (a) Polarization curves for the HER recorded at a sweep rate of 1 mV s^{-1} in 32 mass % NaOH at 90 ^{o}C corrected for the IR drop. Samples: NiSn(10) – (dash); NiSn(30) – (dot); NiSn(60) – (dash-dot); NiSn(100) – (dash-dot-dot); DN – commercial De Nora's electrode (solid). (b) The values of current densities recorded at the potential of -1.2 V, taken from the polarization curves. (c) The values of potentials corrected for the IR drop recorded at j = -0.3 A cm^{-2}, taken from the polarization curves.

Considering the shape of polarization curves it can be seen that the linear Tafel region cannot be detected at all polarization curves. It is generally accepted that the first step in the HER is the Volmer (discharge) reaction which involves the formation of adsorbed hydrogen (H_{ads}) intermediate followed by either the Heyrovsky step, or the Tafel (recombination) step [40,41]. Usually, it is assumed that the forward rate of one of these reaction steps is rate-determining in the overall reaction mechanism. In such a case the HER can be described by linear Tafel relationships and constant reaction orders. However, there is a potential interval in which the overall rate of the HER is under mixed control by the kinetics of the first and the second step. In this case the Tafel relationship is not linear. It is also important to emphasize that the linear Tafel relationship cannot be achieved in the potential region in which the surface coverage by the electroactive intermediate is changing appreciably with potential.

3.2.2. EIS results

The EIS results obtained for all NiSn samples consisted of two overlapping semi-circles. In Fig. 3a are shown Nyquist plots for different samples (A-D) recorded at the same potential (E = -1.23 V), while in Fig. 3b Nyquist plots recorded for sample D at different potentials are presented. Experimental results are presented with squares, circles and triangles, while the fitting results are presented with solid, dashed, dotted and dash-dot lines. All EIS results were fitted with the equivalent circuit shown in Fig. 4, where the parameters were defined as: R_s – solution resistance; R_{ct} – charge transfer resistance; CPE_{dl} – constant phase element for the double layer; R_p and C_p are complex functions of the kinetic parameters. Corresponding results are given in Table 2. Both semi-circles increased with increasing roughnes of the Ni-Sn coatings and content of Ni (Fig. 3a). Similar behavior was observed with the increase of cathodic potential (Fig. 3b). The semi-circle at higher frequencies corresponds to the parameters R_{ct} and CPE_{dl} and the other one at low frequencies corresponds to the parameters R_p and C_p. The value of C_{dl} was determined from the relation [42]:

$$C_{dl} = [Y_{dl}(\frac{1}{R_s} + \frac{1}{R_{ct}})^{(\alpha_{dl}-1)}]^{\frac{1}{\alpha_{dl}}} \quad (1)$$

In Fig. 5a C_{dl} vs. E dependences are shown, while in Fig. 5b E vs. log $(R_F)^{-1}$ dependences are presented for all Ni-Sn samples ($R_F = R_{ct} + R_p$).

The fact that the impedance diagrams consisted of two overlapping semi-circles with the semicircle at the low-frequency end being related to circuit elements R_p and C_p, as well as the change of slope at E vs. log $(R_F)^{-1}$ dependences for each sample, clearly indicates that non-linear Tafel

relationship for the HER at all investigated electrodes is caused by the change of the surface coverage of the H_{ads} intermediate with potential [40,41].

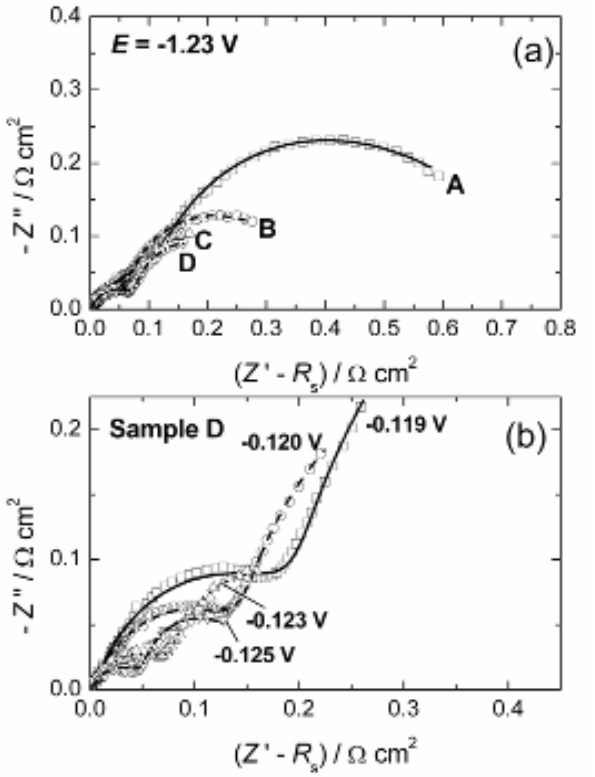

Figure 3 - (a) Nyquist plots for different samples (A-D) recorded at the same potential. (b) Nyquist plots recorded for sample D at different potentials (marked in the figure).

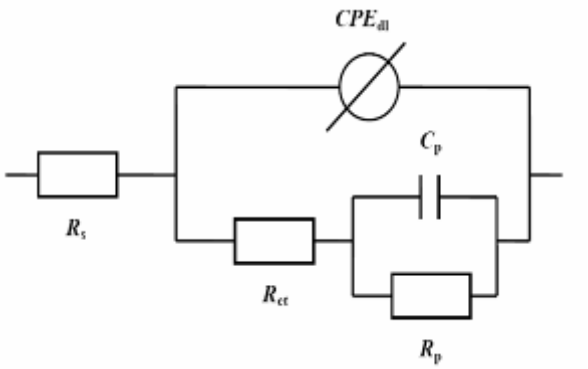

Figure 4 - Equivalent circuit for fitting EIS results: R_s – solution resistance; R_{ct} – charge transfer resistance; CPE_{dl} – constant phase element for the double layer; R_p and C_p are complex functions of the kinetic parameters.

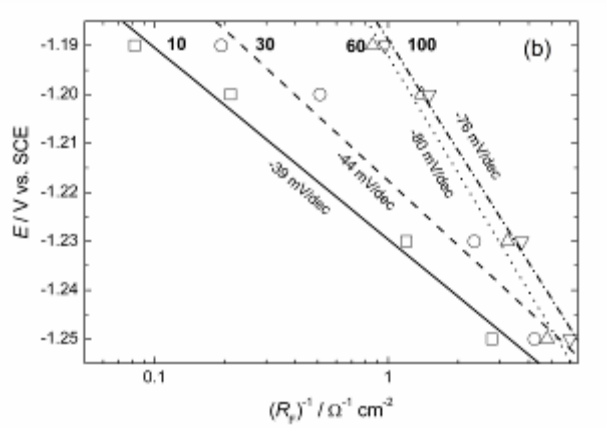

Figure 5 - (a) C_{dl} vs. E dependences. (b) E vs. log $(R_F)^{-1}$ dependences.

3.3. OER

3.3.1. EIS results

EIS spectra recorded successively in the direction of the increasing potential for the most active NiSn100 electrode are presented in the Nyquist complex plane representation in Fig. 6. The Nyquist plots consist of two overlapping distorted semicircles forming an arch. A semicircle obtained in the low frequency region is related to the OER, while semicircle obtained in high frequency range is probably associated with the EIS response of the underlying passive oxide film (inset in Fig. 6 - part of the Nyquist plot marked with square).

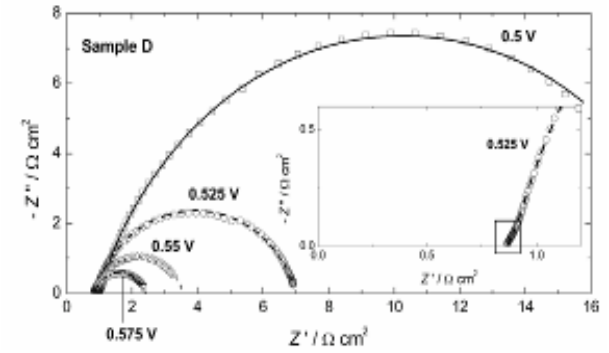

*Figure 6 - Nyquist plots for the OER at sample **D** recorded at different potentials (marked in the figure): Inset – high frequency end showing small semi-circle marked with square.*

Accordingly, impedance data may be simulated in terms of the equivalent circuit shown in Fig. 7a, where R_{ct}, R_p and C_p are potential dependent parameters related to the OER mechanism: C_p denotes the pseudo-capacitance associated with the potential-dependent surface coverage of an adsorbed intermediate in the OER mechanism (OH or O adsorbed species). R_{ox} and C_{ox} are potential independent parameters which appear in the high

frequency range, due to the underlying passive oxide film.

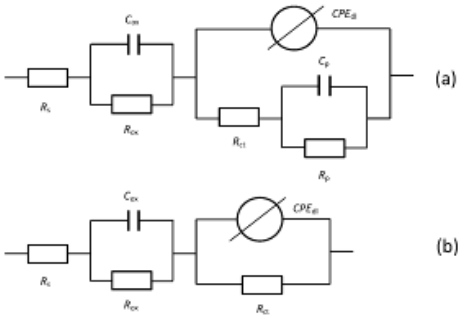

Figure 7 - Equivalent circuits used for fitting EIS results: R_{ct}, R_p and C_p are potential dependent parameters related to the OER mechanism: C_p denotes the pseudo-capacitance associated with the potential-dependent surface coverage of an adsorbed intermediate in the OER mechanism (OH or O adsorbed species). R_{ox} and C_{ox} are potential independent parameters which appear in the high frequency range, due to the underlying passive oxide film.

An additional simplification of the equivalent circuit presented in Fig.7a is possible when $R_p \rightarrow 0$, which is achieved when the surface coverage of an adsorbed intermediate in the OER mechanism is constant in the investigated potential range. Using NLLS fitting procedure the impedance data were fitted with the equivalent circuit model depicted in Fig. 7b.

Since the discussion is restricted to the aspects of the EIS data related to kinetics of the OER and to the roughness factor determination, the corresponding fit values of the equivalent circuit elements related to the OER mechanism are listed in Table 2. The resistive element R_{ct} is related to the kinetics of the interfacial charge transfer reaction and the slope of a plot E vs. log $(R_{ct})^{-1}$ is equal to the Tafel slope, b [19], which is graphically presented in Fig. 8b for all investigated samples. The values of Tafel slopes and other kinetic parameters are given in Table 3.

Table 2 - Parameters of fitting experimentally obtained EIS results using equivalent circuit presented in Fig. 7b and neglecting parameters R_{ox} and C_{ox}.

Sample	E / V vs. SCE	R_s / Ω cm^2	R_{ct} / Ω cm^2	Y_{dl} / Ω^{-1} cm^2 s$^{\alpha}_{dl}$	α_{dl}	C_{dl} / F cm^{-2}	r_{dl}(av.)
Ni	0.500	0.605	35.8	0.00147	0.895	0.00064	1
	0.525	0.605	12.2	0.00127	0.901	0.00057	
	0.550	0.611	4.8	0.00108	0.910	0.00052	
	0.575	0.619	2.6	0.00091	0.921	0.00047	
A	0.500	0.808	23.6	0.02161	0.852	0.01080	17
	0.525	0.804	8.2	0.01951	0.840	0.00873	
	0.550	0.805	3. 5	0.01670	0.854	0.00784	
	0.575	0.828	2.1	0.01569	0.848	0.00671	
B	0.500	0.821	18.1	0.04996	0.886	0.03296	49
	0.525	0.807	9.0	0.04691	0.873	0.02872	
	0.550	0.806	4.2	0.04854	0.820	0.0228	
	0.575	0.816	2.2	0.05004	0.774	0.0172	
C	0.500	0.804	17.5	0.06769	0.911	0.05088	80
	0.525	0.808	6.2	0.06014	0.914	0.04494	
	0.550	0.815	2.6	0.06036	0.891	0.04095	
	0.575	0.822	1.6	0.06299	0.876	0.03983	
D	0.500	0.827	18.4	0.07732	0.956	0.06795	107
	0.525	0.825	6.1	0.06744	0.947	0.05706	
	0.550	0.827	2.6	0.06669	0.926	0.05184	
	0.575	0.838	1.5	0.06850	0.906	0.04874	

Table 3 - Kinetic parameters for the OER at Ni and NiSn electrodes in 1.0 mol dm^{-3} NaOH solution at 25°C.

Sample	Tafel slopes / mV dec^{-1}			j_o / mA cm^{-2}	E / V (j = 100 mA cm^{-2})
	b_1	(EIS)	b_2		
Ni	55	65	259	$8.8 \cdot 10^{-8}$	0.460
A	60	68	152	$1.5 \cdot 10^{-6}$	0.536
B	59	75	139	$2.4 \cdot 10^{-6}$	0.560
C	63	67	144	$6.2 \cdot 10^{-6}$	0.600
D	57	64	133	$7.4 \cdot 10^{-6}$	0.790

The evaluation of the activity of catalysts requires that the electrochemically active surface area (A_{ECSA}) is known. The A_{ECSA} can be determined from the C_{dl} obtained by the analysis of the EIS results using Eqn. (1) (included in Table 2). As can be seen, the values of C_{dl} corresponding to the five electrodes are markedly different (Table 2 and Fig. 8a). The roughness factor can be determined by dividing the C_{dl}, expressed in μF cm^{-2} by 60 μF cm^{-2}, which is assumed to be the order of magnitude of the capacitance of a perfectly flat oxide/electrolyte interface [43]. Although C_{dl} of an electrode can be measured with high precision, its exact value depends on the potential in the processes of hydrogen and oxygen evolution. With increasing current density of OER, C_{dl} decreases due to partial shielding of the electrode surface with oxygen bubbles. So, active surface area of the investigated electrodes, i.e. roughness factors (r_{dl}) were determined as the ratio of the active surface areas of the corresponding NiSn electrodes and Ni electrode, which is equal to the ratio of their double-layer capacitances. The average values of ratios of active surface areas (r_{dl}(av.)) are also given in Table 2.

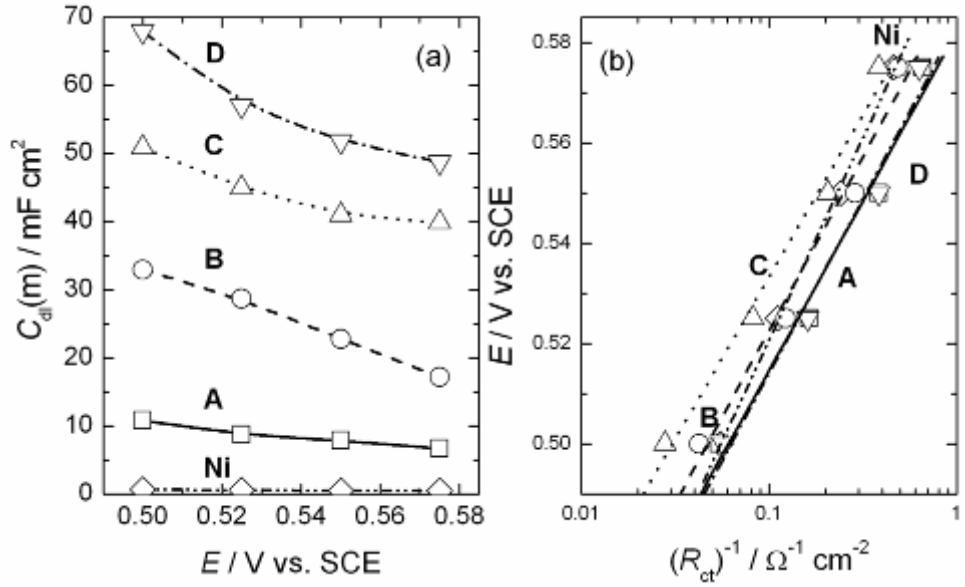

*Figure 8 - (a) Measured values of C_{dl} vs. E for **Ni** and Ni-Sn samples (**A**-**D**). (b) E vs. log $(R_{ct})^{-1}$ dependences for **Ni** and Ni-Sn samples (**A**-**D**).*

3.3.2. Polarization curves

Polarization curves recorded during reverse sweep (from 0.7 V to 0.4 V) for the OER on Ni and Ni-Sn electrodes are shown in Fig. 9. By comparing the polarization curves, which were not corrected for the roughness factor, it can be concluded that the sample **D**, electrodeposited at the highest current density, exhibited the highest catalytic activity for the OER.

Two Tafel slopes for the Ni-Sn samples were observed in the whole potential range studied. Table 3 shows that the Tafel slopes at lower current densities (b_1) were found to vary between 57 and 63 mV dec^{-1} (polarization curves), while the Tafel slope at higher current densities (b_2) was about 120 mV dec^{-1}. In the case of Ni electrode, the corresponding Tafel slopes were 55 mV dec^{-1} at lower current densities and about 259 mV dec^{-1} at high current densities. Chialvo et al. [44] showed that Tafel slope for the OER depended on pre-treatment of Ni electrode. In the low overpotential region Tafel slopes were either 80 or 30 mV dec^{-1}, while in the high overpotential region the Tafel slopes varied between 120 and 190 mV dec^{-1}, depending on pre-treatment of Ni electrodes [44].

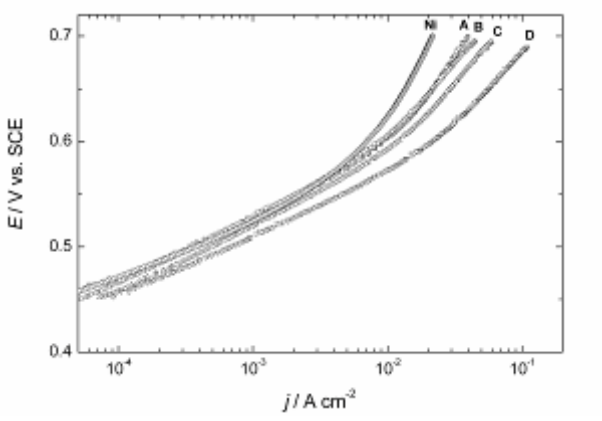

*Figure 9 - Polarization curves recorded during reverse sweep (from 0.7 V to 0.4 V) for the OER on **Ni** and Ni-Sn electrodes (**A**-**D**).*

Besides the well-known difficulties in determining the mechanism of the OER, related to the impossibility of identifying the intermediate species and the fact that 4 electrons are discharged per one molecule of evolved oxygen, formal approach to the study of the kinetics of this reaction on metal oxides is more complicated due to the uncertain values of the stoichiometric number. Determination of stoichiometric numbers is difficult because of poorly defined oxygen reduction reaction on nickel oxides. At potentials at which an oxygen reduction reaction takes place, the reduction of nickel oxide occurs in parallel causing the change of the electrode surface.

Because of these problems, formal approach to the study of the mechanism of the OER is practically impossible. Most of the research is based on the observed values of the Tafel slope and reaction order for OH^- ions in alkaline solutions or H^+ ions in acid solutions under the assumption of Langmuir or Temkin conditions of adsorption.

In a further text the mechanism of the OER on Ni-Sn electrodes will be discussed through general path for the OER on oxide electrodes proposed by Trasatti [4] adopted for alkaline media:

The first steep is the charge-transfer step of the formation of an adsorbed hydroxyl species onto a surface active site M

$$M + OH^- \rightarrow MOH_{ads} + e \qquad (2)$$

The second step can occur through an electrochemical oxide formation path, with a second electron transfer,

$$MOH_{ads} + OH^- \rightarrow MO_{ads} + H_2O + e \qquad (3)$$

or an oxide path with a recombination step

$$MOHads + MOH_{ads} \rightarrow MO_{ads} + H_2O + M \qquad (4)$$

Finally, the formation of O_2 occurs via recombination of two adjacent adsorption sites (third step)

$$2MO_{ads} \rightarrow 2M + O_2\ (g) \qquad (5)$$

From above mechanism, the following Tafel slopes should be detected on the polarization curves: 120 mV dec^{-1} when the overall reaction rate is controlled by the step (2), 40 mV dec^{-1} for step (3), 30 mV dec^{-1} for step (4) and 15 mV dec^{-1}, for step (5).

For a Tafel slope of 60 mV dec^{-1}, obtained at all investigated electrodes, at low current density range, step (2) can be substituted by the following elemental steps:

$$M + OH^- \rightarrow MOH^*_{ads} + e \qquad (2a)$$

$$MOH^*_{ads} \rightarrow MOH_{ads} \qquad (2b)$$

in which adsorption intermediates MOH^*_{ads} and MOH_{ads} possess the same chemical structure but different energy states. Therefore, elemental step (2b) probably controls the overall rate of the OER at low current densities, at both Ni electrode and Ni-Sn electrodes (Tafel slope of 60 mV dec^{-1}). At higher current densities, the overall rate of OER on Ni-Sn electrodes is controlled by a first step (2a) (Tafel slope of 120 mV dec^{-1}). Tafel slope of 259 mV dec^{-1}, obtained on Ni electrode in the high current density range cannot be explained with the formal kinetic approach. As already mentioned previously, the prolonged anodic polarization causes the formation of higher oxides than β-NiOOH, such as NiO_2 [12] and significant decrease of electrical conductivity of Ni oxides film, which assumes the presence of an additional space charge region formed at the electrode/oxide film interface, resulting in additional polarization of electrode.

In order to compare the intrinsic catalytic activity of Ni-Sn electrodes with Ni electrode activity the current density was normalized by r_{dl}, thus eliminating the influence of geometric factor on electrode catalytic activity. Polarization curves with normalized current densities for Ni-Sn samples were almost identical, indicating that all Ni-Sn electrodes exhibited a similar intrinsic catalytic activity and that the highest apparent catalytic activity of sample **D** was due to the most developed electrochemically active surface area. The Ni electrode showed even better intrinsic catalytic activity for the OER than Ni-Sn electrodes.

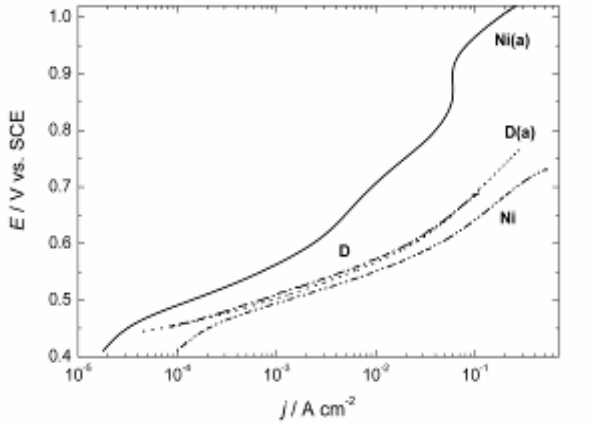

*Figure 10 - Polarization curves for the OER at Ni (**Ni**) and Ni-Sn electrode (**D**) before oxygen evolution at 0.3 A cm^{-2} for 1 h. Polarization curves for the OER at Ni (**Ni(a)**) and Ni-Sn electrode (**D(a)**) after oxygen evolution at 0.3 A cm^{-2} for 1 h.*

The stability of the electrodes was monitored through the impact of previous anodic polarization on their catalytic activity for the OER. The Ni electrode and sample **D** were polarized at a constant current density of 0.3 A cm^{-2} for 1 h and after such pre-electrolysis polarization curves were recorded and presented in Fig. 10. In the case of

Ni electrode pre-electrolysis caused significant decrease of catalytic activity for the OER (increase of potential), **Ni(a)**, while the Ni-Sn electrode, **D(a)**, retained its initial activity.

The increase of overvoltage (decrease of activity) for the OER on Ni anode during the electrolysis of water at a constant current density is a well-known phenomenon. According to thermodynamic data higher nickel oxides can be formed in the potential range where the OER takes place, such as hydrated NiO_2. Some researchers have shown that under above mentioned conditions, further oxidation of NiOOH takes place, forming nickel oxides in which the O/Ni ratios are in the range of 1.7 -1.9. Srinivasan et al. [12] concluded that NiO_2 formation in the oxide film caused a significant decrease of its electronic conductivity and permanent loss of catalytic activity for the OER.

Despite the fact that the best Ni-Sn electrode (**D**) did not exhibit better intrinsic catalytic activity than **Ni**, its high stability during OER and acceptable apparent activity makes it promising anode in alkaline water electrolysis.

4. CONCLUSIONS

(HER): The Ni-Sn alloy coatings were obtained by simple alloy electrodeposition. Their catalytic activity for the HER was higher than that for commercial DN cathode, partially due to increase of electrochemically active surface area and mainly due to formation of catalytically active $Ni_{(1+x)}Sn$ ($0 < x < 0.5$) phase.

(OER): The apparent activities towards the OER of the Ni-Sn coatings are much greater than the one obtained for the Ni electrode, mainly due to an increase in the electrochemically active surface areas. The OER on all investigated Ni-Sn electrodes could be explained by the same reaction mechanism involving OH species adsorbed on the oxide surface. It was also observed that the prolonged anodic polarization led to the loss of the initial catalytic activity of Ni electrode which was explained by further oxidation of NiOOH, and formation of higher nickel oxides at the Ni surface. In contrast, the Ni-Sn electrodes retained their initial activity after prolonged anodic polarization. Ni-Sn electrode prepared by electrodeposition at the highest cathodic current density of -100 mA cm^{-2} exhibited the highest apparent catalytic activity for the OER.

Acknowledgement

The authors are indebted to the Ministry of Education, Science and Technological Development of the Republic of Serbia for the financial support of this work through the project No. 172054.

REFERENCES

[1] M.B.F.Santos, E. Peres Da Silva, R.Andrade Jr, J.A.F.Dias (1992) NiSn and porous NiZn coatings for water electrolysis, Electrochim. Acta, 37, 29-38.

[2] H.Yamashita, T.Yamamura, K.Yoshimoto (1993) The Relation Between Catalytic Ability for Hydrogen Evolution Reaction and Characteristics of Nickel-Tin Alloys, J. Electrochem. Soc., 140, 2238-2246.

[3] V.D.Jović, U.Lačnjevac, B.M.Jović, N.V.Krstajić (2012) Ni-Sn coatings as cathodes for hydrogen evolution in alkaline solution. Chemical composition, phase composition and morphology effects, Int. J. Hydrogen Energy, 37, 17882-17890.

[4] S.Trasatti (1990) Electrode kinetics and electrocatalysis of hydrogen and oxygen electrode reactions. 4. The oxygen evolution reaction, in: H.Wendt (Ed.), Electrochemical Hydrogen Technologies, Elsevier, Amsterdam, p.104.

[5] P.Rasiyah, A.C.C.Tseung, D.B.Hibbert (1982) A mechanistic study of oxygen evolution on $NiCo_2O_4$. I. Formation of higher oxides, J. Electrochem. Soc., 129, 1724-1737.

[6] A.C.C.Tseung, S.Jasem, M.N.Mahmood (1978) Hydrogen Energy System, vol. 1, Pergamon, Oxford, T.N. Veziroglu and W. Seifritz (Eds.), p.215.

[7] S.I.Cordoba, M.Lopez-Teijelo, V.A.Macagno (1987) Voltammetric behaviour of ternary mixtures of Ni, Mn and Fe hydroxides in relation to the oxygen evolution reaction, Electrochim. Acta, 32, 1783-1794.

[8] R.N.Singh, S.K.Tiwari, T.Sharma, P.Chartier, J.F.Koenig (1999) Investigation of oxygen evolution on $LaNi_{1-x}M_xO_3$ (M=Fe, Co, Cu; $0 < x < 0.5$) films of controlled roughness, J. New Mater. Electrochem. Syst., 2, 65-74.

[9] T.Otagawa, J.O'M.Bockris (1982) Lanthanum nickelate as electrocatalyst: oxygen evolution, J. Electrochem. Soc., 129, 2391-2399.

[10] M.H.Miles, G.Kissel, P.W.T.Lu, S.Srinivasan (1976) Effect of temperature on electrode kinetic parameters for hydrogen and oxygen evolution reactions on nickel electrodes in alkaline solutions, J. Electrochem. Soc., 123, 332-341.

[11] P.W.T. Lu, S. Srinivasan (1979) Advances in water electrolysis technology with emphasis on use of the solid polymer electrolyte, J. Appl. Electrochem., 9, 269-278.

[12] P.W.T.Lu, S.Srinivasan (1978) Electrochemical–ellipsometric studies of oxide film formed on nickel during oxygen evolution, J. Electrochem. Soc., 125, 1416-1427.

[13] B.E.Conway, M.A.Sattar, D.Gilroy (1969) Electrochemistry of the nickel-oxide electrode-V. Self-passivation effects in oxygen-evolution kinetics, Electrochim. Acta, 14, 677-685.

[14] R.F.Scarr (1969) The mechanism of oxygen evolution on nickel, platinum, and other metals and alloys, J. Electrochem. Soc., 116, 1526-1535.

[15] S.M.Jasem, A.C.C.Tseung (1979) A potentiostatic pulse study of oxygen evolution on teflon-bonded nickel–cobalt oxide electrodes, J. Electrochem. Soc., 126, 1353-1362.

[16] M.R.Tarasevich, B.N.Efremov (1980) Electrodes of Conductive Metallic Oxides, Elsevier, S. Trasatti (Ed.), Amsterdam, p. 221.

[17] N.Sato, G.Okamoto (1965) Reaction mechanism of anodic oxygen evolution on nickel in sulphate solutions, Electrochim. Acta, 10, 495-506.

[18] B.E.Conway, P.L.Bourgault (1962) Electrochemistry of the nickel oxide electrode: part III. Anodic polarization and self-discharge behavior, Can. J. Chem., 40, 1690-1699.

[19] [19] M.E.G.Lyons, M.P.Brandon (2008) The oxygen evolution reaction on passive oxide covered transition metal electrodes in aqueous alkaline solution. Part 1 - nickel, Int. J. Electrochem. Sci., 3, 1386-1392.

[20] G.Bronoel, J.Reby (1980) Mechanism of oxygen evolution in basic medium at a nickel electrode, Electrochim. Acta, 25, 973-980.

[21] X.Wang, H.Luo, H.Yang, P.J.Sebastian, S.A.Gamboa (2004) Oxygen catalytic evolution reaction on nickel hydroxide electrode modified by electroless cobalt coating, Int. J. Hydrog. Energy, 29, 967-975.

[22] V.S.Bagotzky, N.A.Shumilova, E.I.Khrushcheva (1976) Electrochemical oxygen reduction on oxide catalysts, Electrochim. Acta, 21, 919-927.

[23] J.W.Schultze (1970) Potentiostatische Messungen zur Sauerstoffentwicklung und Oxidschichtbildung an Platinelektroden, Z. Phys. Chem. N.F., 73, 29-38.

[24] D.N.Buckley, L.D.Burke (1976) The oxygen electrode. Part 6.-Oxygen evolution and corrosion at iridium anodes, J. Chem. Soc., Faraday Trans., 1, 72, 2431-2442.

[25] A.C.C.Tseung, S.Jasem (1977) Oxygen evolution on semiconducting oxides, Electrochim. Acta, 22, 31-40.

[26] R.W.Cairns, E.Ott (1934) X-ray studies of the system nickel–oxygen–water. III. The K-absorption limits of nickel in various oxide-hydrates, J. Am. Chem. Soc., 56, 1094-1103.

[27] D.A.Davies, W.Barker (1964) Influence of pH on corrosion and passivation of nickel, Corrosion, 20, 47-55.

[28] J.Balej (1985) Electrocatalysts for oxygen evolution in advanced water electrolysis, Int. J. Hydrog. Energy, 10, 89-96.

[29] S.I.Cordoba, R.E.Carbonio, M.Lopez-Teijelo, V.A.Macagno (1986) The electrochemical response of binary mixtures of hydrous transition metal hydroxides co-precipitated on conducting substrates with reference to the oxygen evolution reaction, Electrochim. Acta, 31, 1321-1332.

[30] S.I.Cordoba, R.E.Carbonio, M.Lopez-Teijelo, V.A.Macagno (1987) The effect of iron hydroxide on nickelous hydroxide electrodes with emphasis on the oxygen evolution reaction, Electrochim. Acta, 32, 749-757.

[31] B.B.Erhov, O.G.Malandin, A.V.Vasev, A.A.Kamnev, G.V.Suchkova (1987) The influence of iron oxyhydroxides on physico-chemical properties of nickel oxide electrode, Elektrokhimiya, 23, 565-574.

[32] J.P.Hoare (1969) The Electrochemistry of Oxygen, Interscience, New York.

[33] L.D.Burke, T.A.M.Twomey (1984) Influence of the acid/base character of the surface on the electrocatalytic behaviour of both nickel and nickel oxide anodes, with particular reference to oxygen gas evolution, J. Electroanal. Chem., 167, 285-294.

[34] J.L.Weininger, M.W.Breiter (1963) Effect of crystal structure on the anodic oxidation of nickel, J. Electrochem. Soc., 110, 484-493.

[35] M.Battaglia, R.Inguanta, S.Piazza, C.Sunseri (2014) Fabrication and characterization of nanostructured Ni-IrO_2 electrodes for water electrolysis, Int. J. Hydrog. Energy, 39, 16797-16806.

[36] G.I.Zakharkin, M.R.Tarasevich, A.M.Khutornoi (1976) Adsorption and electroreduction of molecular oxygen on the metal oxide catalysts, Elektrokhimiya, 2, 1122-1134.

[37] G.Singh, M.H.Miles, S.Srinivasan (1976) Electrocatalysis on Nonmetallic Surfaces (NBS Special Publ. No. 455), U.S. Government Printing Office, A.D. Franklin (Ed.), Washington, p. 289.

[38] A.A.Kamnev, B.B.Ezhov (1992) Electrocatalysis of anodic oxygen evolution at the nickel hydroxide electrode by ferric hydroxo species in alkaline electrolytes, Electrochim. Acta, 37, 607-615.

[39] J.Divisek, H.Schmitz, J.Mergel (1980) Neuartige Diaphragmen und Elektrodenkonstruktionen für die Wasser- und Chloralkali-Elektrolyse, Chem. Ing. Tech., 52, 465-476.

[40] R.D.Armstrong, M.Henderson (1972) Impedance plane display of a reaction with an adsorbed intermediate, J. Electroanal. Chem., 39, 81-92.

[41] D.A.Harrington, B.E.Conway (1987) AC impedance of faradaic reactions involving electrosorbed intermediates – I. Kinetic theory, Electrochim. Acta, 32, 1703-1716.

[42] B.M.Jović, U.Č.Lačnjevac, N.V.Krstajić, V.D.Jović (2014) Service life test of the NiSn coatings as cathodes for hydrogen evolution in industrial chlor-alkali electrolysis, Int. J. Hydrogen Energy, 39, 8947-8959.

[43] D.E.Pissinis, L.E.Sereno, J.M.Marioli (2012) Utilization of special potential scan programs for cyclic voltammetric development of different nickel oxide-hydroxide species on Ni based electrodes, Open J. Phys. Chem., 2, 23-36.

[44] B.Babić, B.Kaluđerović, Lj.Vračar, N.Krstajić (2004) Characterization of carbon cryogel synthesized by sol–gel polycondensation and freeze-drying, Carbon, 42, 2617-2629.

IZVOD

ELEKTROHEMIJSKI ISTALOŽENE Ni-Sn PREVLAKE KAO ELEKTROKATALIZATORI ZA REAKCIJE IZDVAJANJA VODONIKA I KISEONIKA U ALKANIM RASTVORIMA

Reakcija izdvajanja vodonika i kiseonika ispitivana je na čistom Ni i elektrohemijski istaloženim prevlakama Ni-Sn legura različitog sastava i morfologije. Sve prevlake istaložene su na podlozi od Ni mrežice (finoće 40 mesh-a) iz elektrolita koji je sadržao Ni i Sn jone u prisustvu pirofosfata i glicina. Elektrode su ispitivane skenirajućom elektronskom mikroskopijom (SEM), energetski disperzivnom spektroskopijom X zračenja (EDS), metodom impedansne spektroskopije (EIS) i snimanjem polarizacionih dijagrama.

Pokazano je da je pored porasta hrapavosti elektrodnih površina na Ni-Sn legurama sa porastom gustine struje taloženja, promena sastava prevlaka takođe odgovorna za povećanje njihovih katalitičkih osobina za izdvajanje vodonika i kiseonika.

U oblasti potencijala izdvajanja vodonika nije bilo moguće detektovati linearnu zavisnot potencijala od logaritma gustine struje (Tafelov nagib) zbog promene pokrivenosti elektrodne površine sa elektroaktivnim intermedijarnim česticama u funkciji potencijala, ali je pokazano da su Ni-Sn elektrode aktivnije za reakciju izdvajanja vodonika od komercijalne Ni-RuO_2 (DN) elektrode pri gustinama katodne struje većim od 0.3 A cm^{-2}.

Izdvajanje kiseonika je okarakterisano sa dva Tafelova nagiba kod svih ispitivanih elektroda: 60 mV po dekadi pri manjim gustinama struje (do 20 mA cm^{-2}) i 120 mV po dekadi pri većim gustinama struje. Pokazano je da je katalitička aktivnost Ni-Sn elektroda posledica povećanja elektrohemijski aktivne površine. Međutim, ove elektrode ne gube katalitičku aktivnost pri dugotrajnom izdvajanju kiseonika (što je slučaj sa Ni elektrodama), jer se na njihovim površinama ne stvara slabo provodni sloj NiO_2.

Na osnovu Tafelovih nagiba i rezultata impedansnih ispitivanja predloženi su i diskutovani mehanizmi reakcija izdvajanja vodonika i kiseonika.

***Ključne reči**: Izdvajanje H_2, izdvajanje O_2, alkalni rastvor, elektrohemijski istaložene Ni-Sn legure.*

Naučni rad
Rad primljen: 25. 11. 2015.
Rad prihvaćen: 15. 01. 2016.
Rad je dostupan na sajtu: www.idk.org.rs/casopis